China Ocean Eng., Vol. 28, No. 6, pp. 749 – 760

DOI 10.1007/s13344-014-0058-8, ISSN 0890-5487

Hydrodynamic Performance of the Arc-Shaped Bottom-Mounted Breakwater*

CHU Yu-chuan (楚玉川), CHENG Jian-sheng (程建生)[1], WANG Jing-quan (王景全),

LI Zhi-gang (李志刚) and JIANG Ke-bin (江克斌)

College of Field Engineering, *PLA University of Science & Technology*, *Nanjing 210007*, *China*

(Received 7 January 2014; received revised form 30 May 2014; accepted 18 June 2014)

ABSTRACT

The problem of the hydrodynamic interaction with the arc-shaped bottom-mounted breakwaters is investigated theoretically. The breakwater is assumed to be rigid, thin, impermeable and vertically located in a finite water depth. The fluid domain is divided into two sub-regions of inner and outer by an auxiliary circular interface. Linear theory is assumed and the eigenfunction expansion approach is used to determine the wave field. In order to examine the validity of the theoretical model, the analytical solutions are compared to agree well with published results with the same parameters. Numerical results including wave amplitude, surge pressure, and wave force are presented with different model parameters. The major factors including wave parameters, structure configuration, and water depth that affect the surge pressure, wave forces, and wave amplitudes are discussed and illustrated by some graphs and cloud maps.

Key words: *arc-shaped*; *wave diffraction*; *hydrodynamic performance*; *oblique incidence*

1. Introduction

Coastal structures are extensively constructed to withstand the dynamic action of waves and to dissipate their wave energy. They also act as barriers and create a condition of tranquility on the shore side for smooth conduct of the loading and unloading of passengers and cargo. The prediction of the performance of the interactions between water waves and the structures has received considerably much attention from the designers. The arc-shaped bottom-mounted breakwater (ABBW for short) is one type of them, namely a kind of breakwater in concept, whose horizontal section is an arc form, and is usually fixed on the bottom of the water, surface-piercing, impermeable and extended to above the free surface of the water.

Many scholars have researched into the problem of wave interaction performance of different type structures. Garrett (1971) solved the diffraction problem for a single truncated circular dock. Spring and Monkmeyer (1974) investigated the pressures and forces on stationary groups of circular cylinders and proposed the method of matched eigenfunction expansion which was further modified by Linton and Evans (1990). Zhu and Moule (1994) found that large forces on an elliptical cylinder compared with those induced by plane waves with the same total wave number can be induced by linear

* This project was financially supported by the Major State Basic Research Development Program of China (973 Program, Grant Nos. 2014CB046801 and 2014CB046804) and the Foundation of the China Scholarship Council (Grant No. 201203170143).

1 Corresponding author. E-mail: coussinesq@126.com

short-crested waves, and discussed the wave force of a vertical cylinder of arbitrary cross-section by the boundary element method. Williams and Li (2000) theoretically investigated the interaction of water waves with arrays of surface-piercing, bottom-mounted circular cylinders by the eigenfunction expansion approach. Bhatta and Rahman (2003) derived analytical and numerical results for the wave loads on a floating circular cylinder heaving in water of finite depth in the presence of an incident wave. Sankarbabu *et al.* (2008) investigated the hydrodynamic performance of a dual cylindrical caisson breakwater (DCBW) formed by a row of caissons each of which consisting of a porous outer cylinder circumscribing an impermeable inner cylinder with the eigenfunction expansion method. Song and Tao (2007) carried out to investigate the general 3D short-crested wave interaction with a concentric two-cylinder system and derived the analytical solution based on linear potential theory. Liu *et al*. (2012) and Liu and Lin (2013) extended the SBFEM which combines the advantages of the finite element method and the boundary element method to research the short-crested wave interaction with a concentric cylindrical structure with different types of inner and outer walls.

Nevertheless, there are relatively limited theoretical studies on the interaction between the water wave and the structures which have relative special section, such as V-shaped and arc-shaped breakwaters. Lu *et al.* (2007) obtained an analytical solution of the force exerting on the V-shaped breakwater, while gave the solution related with water depth and breakwater parameters and so on. Chang *et al.* (2012) proposed a modified V-shaped model and presented an accurate solution to diffraction around it by a semi-analytic method. The reflection and transmission properties of a submerged circular arc plate were studied in deep water by McIver and Urka (1995). Kanoria and Mandal (2002) investigated the problem of wave scattering around two symmetric circular-arc-shaped thin plates submerged in deep water by the method of hypersingular integral equations which are solved approximately using finite series involving Chebyshev polynomials of the second kind. Miao *et al.* (2005), Cheng *et al.* (2006, 2007, 2008) and Duan *et al.* (2012) studied the wave interaction with different kinds of arc-shaped and V-shaped breakwaters by an analytic method, and they have focused on the characteristics of the wave diffraction around the structures in wave fields without reference to the hydrodynamic pressure and force.

In this paper, the analytical model with the inclusion of multiple interactions between the plane wave and the ABBW is presented based on the theory research of Miao *et al.* (2005) and Cheng *et al.* (2008). The characteristics of the wave diffraction including the wave amplitude and the hydrodynamic force are investigated under different configures as a perfection and extension. The analytical solution is obtained by the approach of the eigenfunction expansion and sub-fluid region matching on the artificial circular interface under the assumption of the linear wave theory. The reliability of the presented solution is validated by comparing with the available published results under taking the same parameters of the calculated model. The hydrodynamic pressure and the wave force on the surface of the breakwater and wave amplitude around the breakwater under the interaction with plane waves are shown and the change rules of the results are herein discussed. The effects of a range of incident wave parameters and structural configurations on the hydrodynamic force on the breakwater and wave elevation in wave field are brought out in a more detailed elaboration.

2. Theoretical Formulation and Solution

The geometric layout of the problem is shown in Fig. 1. A vertical, bottom-mounted, surface-piercing, arc-shaped breakwater of radius R is vertically fixed in water of uniform depth d. The upright wall of breakwater is regarded rigid, thin and impermeable. A Cartesian coordinate system (x, y, z) is defined with the origin at the still water surface and the z-axis directing vertically upwards through the arc center. The x-axis is defined to make the breakwater located between $\alpha \leq \theta \leq 2\pi-\alpha$, and θ is measured counterclockwise from the positive x-axis. The corresponding central angle of the ABBW is $\gamma = 2\pi-2\alpha$. The problems are considered herein in the cylindrical polar coordinate system (r, θ, z). The breakwater is subjected to a train of regular, monochromatic, incident waves of small amplitude A, frequency ω and wave length L propagating at an angle β to the positive x-axis.

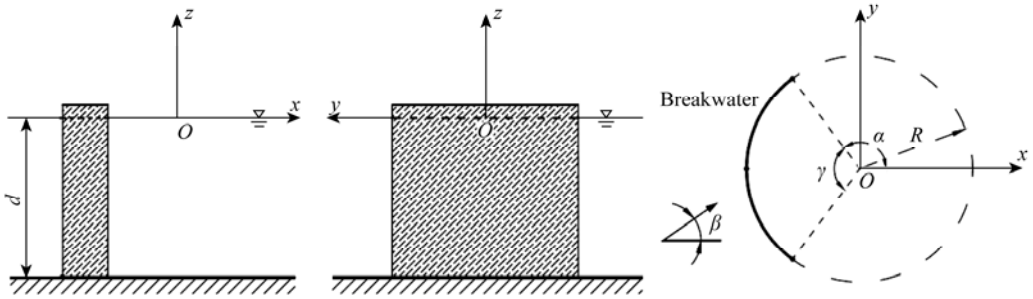

Fig. 1. Breakwater and coordinate system.

Under the assumption of linear water wave theory, the small amplitude, irrotational motion of the inviscid, incompressible fluid may be described in terms of velocity potential $\Phi(r, \theta, z, t)$. The fluid domain is divided into two regions: Z_1: ($r \geq R$, $0 \geq z \geq -d$), Z_2: ($R \geq r \geq 0$, $0 \geq z \geq -d$) by the auxiliary cylindrical interface ($r=R$). Thus, the velocity potentials $\Phi_j(r, \theta, z, t)$ in each region can be written as:

$$\Phi_j(r, \theta, z, t) = \mathrm{Re}\left[\phi_j(r, \theta, z)\, \mathrm{e}^{-\mathrm{i}\omega t}\right],\ j = 1,\ 2, \tag{1}$$

in which Re[ ] denotes the real part of a complex expression, ϕ_j (for j=1, 2 corresponding to the region Z_1 and Z_2) is the spatial velocity potential which satisfies the Laplace equation given by

$$\frac{\partial^2\phi_j}{\partial r^2}+\frac{1}{r}\frac{\partial\phi_j}{\partial r}+\frac{1}{r^2}\frac{\partial^2\phi_j}{\partial\theta^2}+\frac{\partial^2\phi_j}{\partial z^2}=0,\ j=1,\ 2. \tag{2}$$

The linearized free surface boundary condition

$$\frac{\partial\phi_j}{\partial z}-\frac{\omega^2}{g}\phi_j=0,\ \text{at}\ z=0,\ j=1,\ 2. \tag{3}$$

The boundary condition at the seabed

$$\frac{\partial\phi_j}{\partial z}=0,\ \text{at}\ z=-d,\ j=1,\ 2. \tag{4}$$

The outer region Z_1 satisfies the radiation boundary condition given by

$$\lim_{r\to\infty}\sqrt{r}\left[\frac{\partial(\phi_1-\phi_I)}{\partial r}-\mathrm{i}k(\phi_1-\phi_I)\right]=0, \tag{5}$$

where ϕ_I is the incident wave potential, i is the square root of −1, k is the real positive root of dispersion relation $\omega^2=gk\tanh(kd)$, ω is the angular frequency, and g is the acceleration of gravity.

Using the method of separation of variables and eigenfunction expansions, we can derive formal solutions of the potentials with unknown coefficients for both regions Z_1 and Z_2.

$$\begin{aligned}\phi_1&=\phi_I+\phi_D\\&=\frac{\cosh\left[k(z+d)\right]}{\cosh(kd)}\sum_{m=0}^{\infty}\left\{\left[E_m\mathrm{J}_m(kr)+A_m\mathrm{H}_m^{(1)}(kr)\right]\cos(m\theta)\right.\\&\left.+\left[F_m\mathrm{J}_m(kr)+B_m\mathrm{H}_m^{(1)}(kr)\right]\sin(m\theta)\right\},\end{aligned} \tag{6}$$

$$\phi_2=\frac{\cosh\left[k(z+d)\right]}{\cosh(kd)}\sum_{n=0}^{\infty}\left[C_n\mathrm{J}_n(kr)\cos(n\theta)+D_n\mathrm{J}_n(kr)\sin(n\theta)\right], \tag{7}$$

where $E_0=\dfrac{Ag}{\mathrm{i}\omega}$, $F_0=0$ for m=0; $E_m=2\mathrm{i}^m\dfrac{Ag}{\mathrm{i}\omega}\cos(m\beta)$, $F_m=2\mathrm{i}^m\dfrac{Ag}{\mathrm{i}\omega}\sin(m\beta)$ for $m\geq1$; A_m, B_m, C_n and D_n are unknown coefficients; $\mathrm{J}_m(kr)$ and $\mathrm{J}_n(kr)$ are the m-th (or n-th) order Bessel functions of the first kind; and $\mathrm{H}_m^{(1)}(kr)$ denotes the m-th order Hankel function of the first kind.

The unknown coefficients can be obtained by the matching conditions at the common imaginary boundary of these two sub-regions. The continuity of normal velocity and pressures at the common auxiliary interface (r=R) is given by

$$\phi_1=\phi_2,\ \text{at}\ r=R,\ -\alpha\leq\theta\leq\alpha, \tag{8}$$

$$\frac{\partial\phi_1}{\partial r}=\frac{\partial\phi_2}{\partial r},\ \text{at}\ r=R,\ -\alpha\leq\theta\leq\alpha, \tag{9a}$$

$$\frac{\partial\phi_1}{\partial r}=\frac{\partial\phi_2}{\partial r}=0,\ \text{at}\ r=R,\ \alpha\leq\theta\leq2\pi-\alpha. \tag{9b}$$

The velocity potential ϕ_1 is composed of the incident wave potential ϕ_I and the diffraction wave potential ϕ_D in the exterior region Z_1, and therefore, ϕ_1 and ϕ_2 in two sub-regions Z_1 and Z_2 can be expressed, respectively, as follows.

Eqs. (9a) and (9b) can be merged as:

$$\frac{\partial\phi_1}{\partial r}=\frac{\partial\phi_2}{\partial r},\ \text{at}\ r=R,\ 0\leq\theta\leq2\pi. \tag{9c}$$

Substituting Eqs. (6) and (7) into Eq. (9c) yields

$$\begin{aligned}&k\sum_{m=0}^{\infty}\left\{\left[E_m\mathrm{J}'_m(kR)+A_m\mathrm{H}'_m(kR)\right]\cos(m\theta)+\left[F_m\mathrm{J}'_m(kR)+B_m\mathrm{H}'_m(kR)\right]\sin(m\theta)\right\}\\&\quad=k\sum_{n=0}^{\infty}\left[C_n\mathrm{J}'_m(kR)\cos(n\theta)+D_n\mathrm{J}'_n(kR)\sin(n\theta)\right].\end{aligned} \tag{10}$$

As the angle θ is arbitrary, we may obtain the following equations from Eq. (10),

$$A_m\mathrm{H}'_m(kR)+E_m\mathrm{J}'_m(kR)=C_n\mathrm{J}'_n(kR),\ m=n=0,\ 1,\ 2,\ldots,\infty; \tag{11}$$

$$B_m \mathrm{H}'_m(kR) + F_m \mathrm{J}'_m(kR) = D_n \mathrm{J}'_n(kR),\ m = n = 0,\ 1,\ 2,..., \infty \tag{12}$$

for the matching conditions Eq. (8) and the impermeable condition Eq. (9b) at the breakwater surface. By taking the similar approach as above, substituting Eqs. (6) and (7) into Eq. (8) and Eq. (9b) yields

$$\sum_{m=0}^{\infty}\left\{\left[E_m \mathrm{J}_m(kR) + A_m \mathrm{H}_m(kR)\right]\cos(m\theta) + \left[F_m \mathrm{J}_m(kR) + B_m \mathrm{H}_m(kR)\right]\sin(m\theta)\right\}$$
$$-\sum_{n=0}^{\infty}\left[C_n \mathrm{J}_n(kR)\cos(n\theta) + D_n \mathrm{J}_n(kR)\sin(n\theta)\right] = 0,\ \text{ at } r = R,\ -\alpha \le \theta \le \alpha, \tag{13}$$

$$k\sum_{n=0}^{\infty}\left[C_n \mathrm{J}'_n(kR)\cos(n\theta) + D_n \mathrm{J}'_n(kR)\sin(n\theta)\right] = 0,\ \text{at } r = R,\ \alpha \le \theta \le 2\pi - \alpha\ . \tag{14}$$

By utilizing the orthogonality characteristics of $\cos(m\theta)$ and $\sin(m\theta)$ over $[0, 2\pi]$, multiplying both sides of Eqs. (13) and (14) by the proper $\sin(t\theta)$, $\cos(t\theta)$ functions, and integrating over the corresponding ranges, it is,

$$\sum_{m=0}^{\infty}\left[E_m \mathrm{J}_m(kR) + A_m \mathrm{H}_m(kR)\right]P_{mt} - \sum_{n=0}^{\infty} C_n\left[\mathrm{J}_n(kR)P_{nt} - k\mathrm{J}'_n(kR)\hat{P}_{nt}\right] = 0\,; \tag{15}$$

$$\sum_{m=1}^{\infty}\left[F_m \mathrm{J}_m(kR) + B_m \mathrm{H}_m(kR)\right]Q_{mt} - \sum_{n=1}^{\infty} D_n\left[\mathrm{J}_n(kR)Q_{nt} - k\mathrm{J}'_n(kR)\hat{Q}_{nt}\right] = 0, \tag{16}$$

where,

$$P_{mt} = \int_{-\alpha}^{\alpha}\cos(m\theta)\cos(t\theta)\mathrm{d}\theta,\ P_{nt} = \int_{-\alpha}^{\alpha}\cos(n\theta)\cos(t\theta)\mathrm{d}\theta,\ \hat{P}_{nt} = \int_{\alpha}^{2\pi-\alpha}\cos(n\theta)\cos(t\theta)\mathrm{d}\theta,$$
$$Q_{mt} = \int_{-\alpha}^{\alpha}\sin(m\theta)\sin(t\theta)\mathrm{d}\theta,\ Q_{nt} = \int_{-\alpha}^{\alpha}\sin(n\theta)\sin(t\theta)\mathrm{d}\theta,\ \hat{Q}_{nt} = \int_{\alpha}^{2\pi-\alpha}\sin(n\theta)\sin(t\theta)\mathrm{d}\theta.$$

The unknown coefficients A_m, B_m, C_n and D_n can be obtained by solving a set of linear algebraic equations from Eqs. (11), (12), (15), and (16).The infinite series are truncated at number M for all the series which determines the order of equations. We may obtain velocity potential everywhere in the fluid domain after obtaining the unknown coefficients.

Thus, the hydrodynamic pressure can be solved by the linearized Bernoulli equation as $p = \mathrm{i}\omega\rho\phi(r, \theta, z)$, where ρ is the fluid density. The wave exciting force and moment on the ABBW in the two orthogonal directions in the x-y plane, F_x, F_y are obtained by the integration of the pressure on the inside and outside wetted surface, expressions are given by

$$\begin{bmatrix} F_x \\ F_y \end{bmatrix} = -\mathrm{i}\omega\rho R\int_{-d}^{0} g(z)\mathrm{d}z\int_{\alpha}^{2\pi-\alpha}\left[\varphi_1(R,\theta) - \varphi_2(R,\theta)\right]\begin{bmatrix}\cos\theta \\ \sin\theta\end{bmatrix}\mathrm{d}\theta, \tag{17}$$

in which $g(z) = \cosh[k(z+d)]/\cosh(kd)$, $\varphi(r, \theta)$ is defined from $\phi(r, \theta, z) = g(z)\varphi(r, \theta)$.

Similarly, the exciting moment M_b on the ABBW about sea-bottom is given by

$$M_\mathrm{b} = -\mathrm{i}\omega\rho R\int_{-d}^{0}(z+d)g(z)\mathrm{d}z\int_{\alpha}^{2\pi-\alpha}\left[\varphi_1(R,\theta) - \varphi_2(R,\theta)\right]\mathrm{d}\theta. \tag{18}$$

3. Numerical Results and Discussion

3.1 Verification

In this section, a computer program is developed to implement the above analysis and the characteristics of hydrodynamic pressure, force and wave elevation for several configurations are

studied. The correctness of the theoretical model and the computer program is tested by comparing with the solution of the open literature. In all numerical examples and figures, the configuration of the breakwater is illustrated in Fig. 1, and the wave amplitudes, hydrodynamic pressures and hydrodynamic forces are nondimensionalized by $|\eta|= \eta/A$, $|P|= p/(\rho gA)$, and $|F|= F/(\rho gAR^2)$.

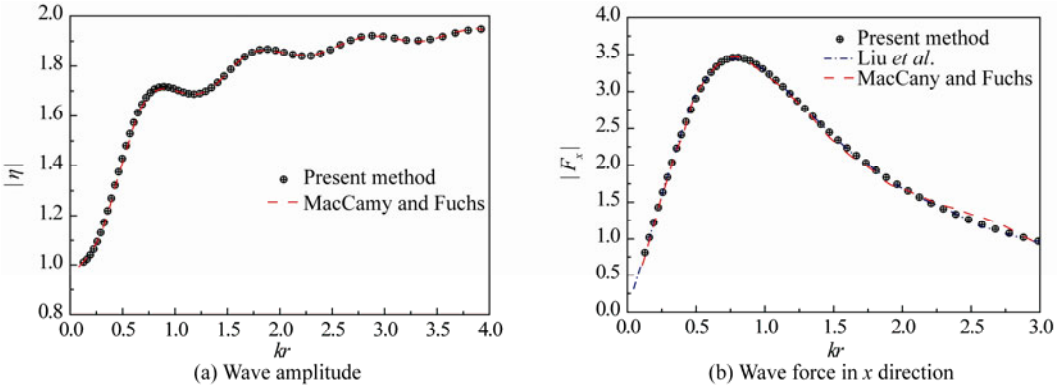

Fig. 2. Validation of the present model with γ=360°.

It is obvious that the solution of the present method covers the results of the large single vertical cylinder when the ABBW opening angle γ=360°. Fig. 2a shows the wave amplitude of both the present solution and the result of MacCamy and Fuchs (1954) at the wave-side outside the breakwater, and Fig. 2b presents the horizontal force exerted on breakwater obtained from the analytic model of MacCamy and Fuchs (1954) and SBFEM model of Liu *et al.* (2012) comparison with the present solution, where the wave amplitude and the force are varied by the relative wave number kr. For matching the examples, parameter values are chosen as the water depth and the radius of breakwater ratio d/r=1.0, the plane waves normalize incident with an angle β=0°, wave amplitude A=1.0 m. As we can see from Figs. 2a and 2b, the present method has a good agreement with the published results, and the correctness of the present theory is verified. It is also found that taking the truncated number M=20 in Eqs. (11), (12), (15) and (16) for calculations appearing herein can obtain sufficient accuracy by the comparison.

3.2 Effect of the Radius Angle γ and the Relative Ratios d/R of the ABBW

In order to investigate the performance of the breakwater, it is interesting to study the changes in the wave surface elevation in the inner and outer region of the artificial boundary for varying incident wave parameters and structure configuration. Fig. 3 shows the wave amplitude distribution around the ABBW from incident wave interaction with the breakwater for configuration parameters: A=1.0 m, d=20.0 m, R=100.0 m, L=25.0 m, β=0°, and the different angles γ=60°, 120°, 360°. As can be seen in Fig. 3, the effect of different opening angles of the breakwater on the wave diffraction is illustrated clearly that the diffracted wave amplitude decreases with the increase of radius angle, and the transmission phenomena is much more obvious for a small γ. It can be summarized that the angle γ has significant effect on wave elevation in the diffracted field, and the ABBW with a large γ has the better

sheltering effects.

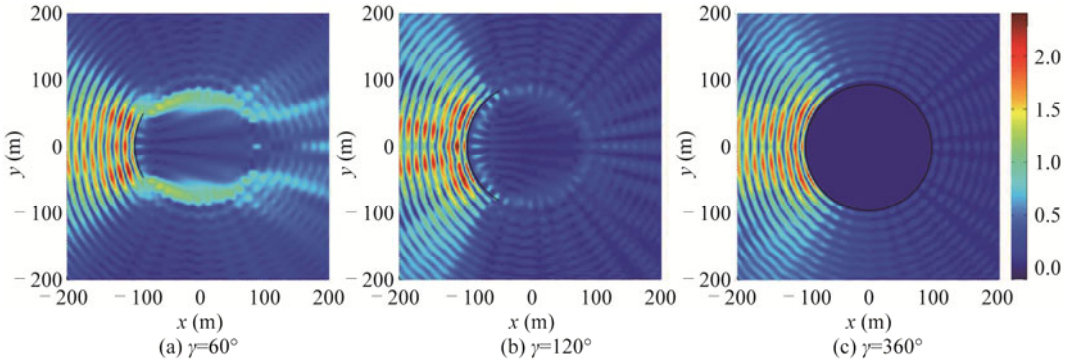

Fig. 3. Diffracted wave amplitude distribution with different radius angles γ.

To obtain better illustration of the distribution of the hydrodynamic pressure on the surface of breakwater, Fig. 4 shows the wave pressure distribution on the whole surface of the ABBW inner and outer resulted from the wave propagation. We only illustrate the hydrodynamic pressure here for simplicity and choose the same parameters as Fig. 3b except for kd=1.0. As clearly shown in Fig. 4, there are similar distribution characteristics for hydrodynamic pressure between the inside and outside on the surface of the structure. The value of hydrodynamic pressure that the cloud maps present is larger near the free surface than that in the deep; what is more, the values also have close relationship with the location angle θ which can be observed in the velocity potential expressions. By comparing the two maps each other, there is an obvious characteristic that $|P_{out}|$ is much higher than $|P_{in}|$ at the same position.

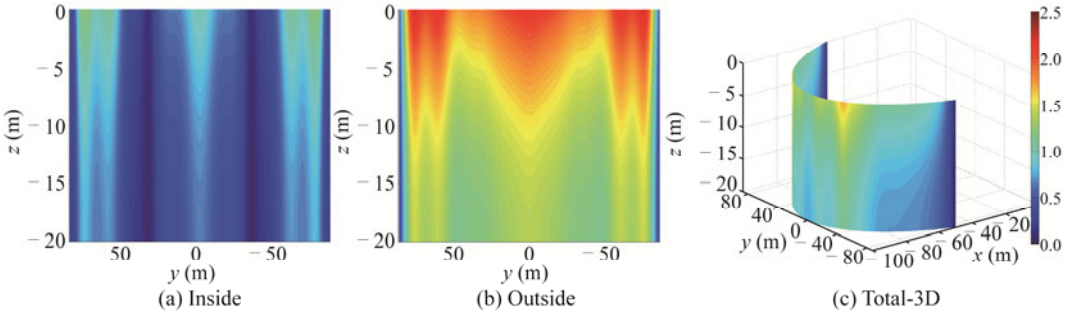

Fig. 4. Dimensionless hydrodynamic pressure on the surface of ABBW.

The variation of the dimensionless wave amplitude $|\eta|$ at the origin O and the horizontal wave forces $|F_x|$ on the ABBW versus the relative wave number kd (from 0.0 to 5.0) for different radius angles are shown in Fig. 5, and setting d=20.0 m, R=100 m in Figs. 5a and 5b. Fig. 5a presents the results of the dimensionless wave amplitudes at the origin O for different radius angles of the ABBW (γ=60°, 120°, 180°, 360°) in the sheltered region. It is clearly seen that the variation of wave amplitudes versus kd and the general trend of the curves oscillates and decreases with the increasing kd for different γ except for the case of γ=360° in which the inner fluid section is completely separated

from the outer wave field by the ABBW. The wave amplitude $|\eta|$ at the origin oscillates nearby between the minimum and the maximum as kd increases, and the wave amplitude $|\eta|$ is larger with a smaller γ than that with a larger γ at the same kd. Fig. 5b plots the total horizontal wave forces variation versus the relative wave number kd on the ABBW. It shows that the horizontal wave forces are quite different for varying γ values and smaller wave force with a smaller γ, but it does not mean that γ is larger and the force is larger, such as γ=360°. In these cases, the maximum and the minimum of $|F_x|$ are corresponding to γ=180° and 60°, respectively. By observing and comparing these cases, it is concluded that the horizontal force $|F_x|$ increases monotonously at first until it reaches the maximum, and then it decreases as kd increases. The change rule of the wave forces is similar to that of the cylinder in the former validation part.

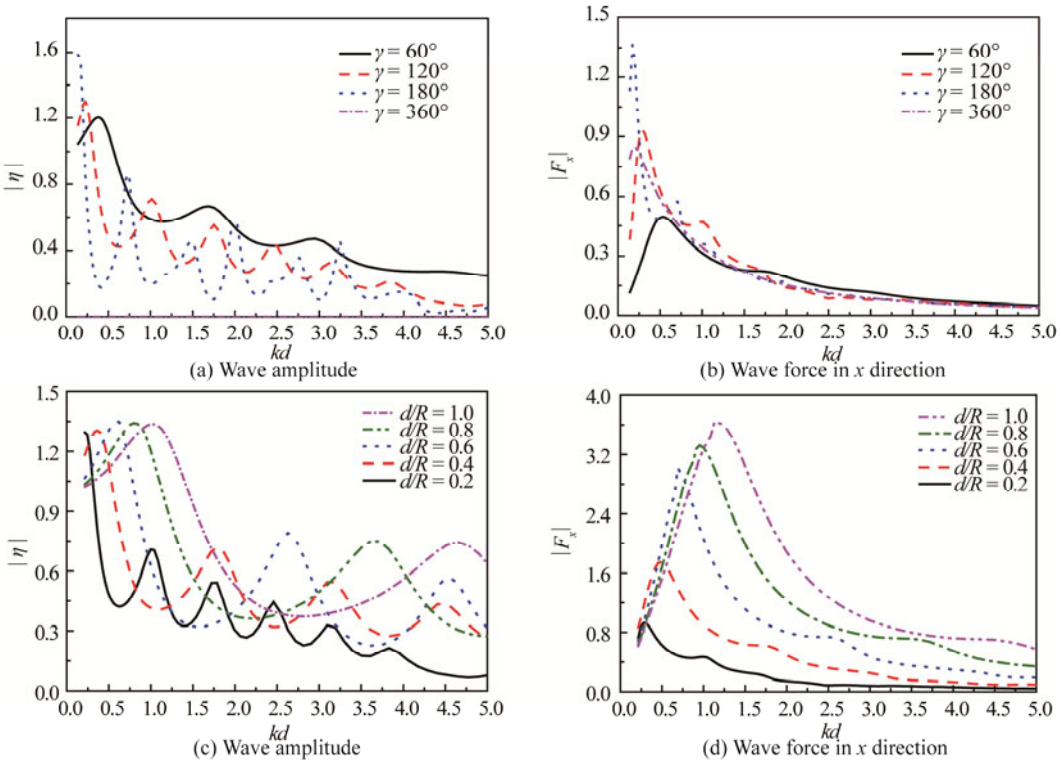

Fig. 5. Variation of the wave amplitudes at the origin and wave forces on the ABBW versus kd.

By setting the opening angle of the ABBW γ=120° in Figs. 5c and 5d, the results of the dimensionless wave amplitudes at the origin O are given in Fig. 5c for different relative water depth ratios (d/R=0.2, 0.4, 0.6, 0.8, 1.0) in the sheltered region. It is clearly seen that the variation of wave amplitudes versus kd and the trend of the curves oscillates and decreases sharply with the increasing kd for different ratios d/R. In addition to the general trend of decreasing wave amplitude, there are troughs for all ratios plotted indicating extremely small wave amplitudes. At low ratios, the curve values remain relatively smaller and oscillation is more obvious than that in other cases. In Fig. 5d, the total horizontal wave forces are shown in the same way. It indicates that the horizontal wave forces are quite

different for varying d/R values and smaller wave force with smaller ratio. Also, the variation of the force is similar among the five ratios and the force increases monotonously for small kd up to about 0.3, 0.5, 0.8, 1.1 and 1.3 corresponding to the maximums of these curves, beyond which, it decreases rapidly with the increasing kd. It is interesting to observe that, for a given value, the wave amplitude at the origin reaches the peak for the first time at a value of kd, meanwhile the horizontal force reaches the maximum near the value of kd.

3.3 Effect of the Angle of Wave Incidence β

Fig. 6 gives the wave amplitude distributions in fluid domain with different directions of wave incidence angle β=30°, 60°, 90°, meanwhile, setting the other parameters the same as that in the case of Fig. 3b. It is clearly seen in Fig. 6 that the wave amplitude distributions are quite different for different β, and it is also concluded that there is a close relationship between $|\eta|$ in the sheltered area and the wave incidence angle β. For small β, the wave reflection is relative apparently and the wave amplitude of the sheltered area is smaller than that for large β.

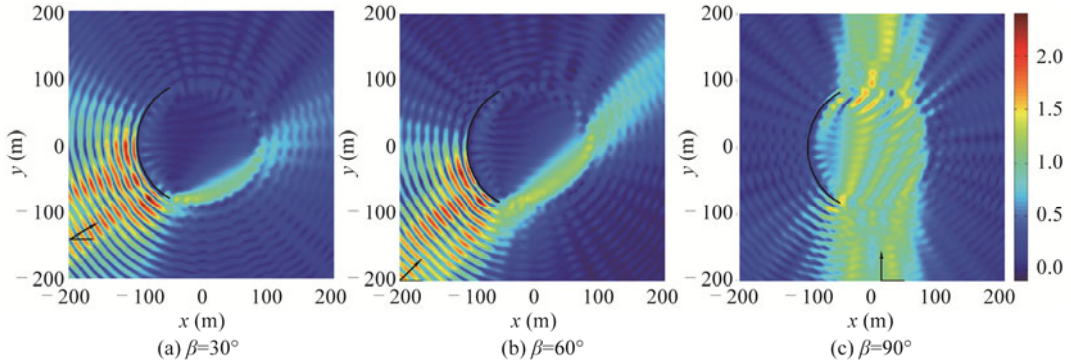

Fig. 6. Diffracted wave amplitude distribution with different angles of wave incidence β.

In Fig. 7, it is of similar performance to Fig. 3 that the cloud maps of wave pressure on the whole surface of ABBW inside and outside are displayed with kd=1.0 and setting the other conditions the same as Fig. 6b. From Figs. 7a and 7b, similar laws of variation between $|P_{in}|$ and $|P_{out}|$ are obtained and the values of hydrodynamic pressure are larger near the free surface than those in the deep, and there is a very close relationship between $|P_{in}|$, $|P_{out}|$ and the locational angle θ, wave incidence angle β, while $|P_{in}|$ is much smaller than $|P_{out}|$ at the same position through comparison. More than that, also we can see different performances of hydrodynamic pressure by comparing the results with those in Fig. 3. The results are asymmetry and larger values concentrate on the right upper of the surface. By the analysis, we can conclude that the angle between the wave incidence direction and the normal of the curved surface of the breakwater is smaller, the values of $|P_{in}|$ and $|P_{out}|$ are larger, and vice versa.

Fig. 8 shows the variation of the dimensionless wave amplitude $|\eta|$ at the origin O and the horizontal wave forces $|F_x|$ on the ABBW versus kd (from 0.0 to 5.0) for β=0°, 30°, 45°, 60°, 90°, and the other parameters are the same as that in Fig. 6. It is restricted to the length of the article, and we do not present the plot of $|F_y|$ herein and the change rule of its values can be obtained easily by the same way as $|F_x|$. It is clearly seen in Fig. 8a, the wave amplitude $|\eta|$ at the origin decreases at first as kd

increases, except for the case of β=90°, and it oscillates nearby between the minimum and the maximum. For the wave incidence angle β=90°, the curve also has an oscillating feature and the oscillatory amplitude decays with the increasing kd, but there is no apparent trend up or down by comparing with other cases. In general, the wave amplitude $|\eta|$ increases as the wave incidence angle β increases, and the characteristic is not obvious in cases of relatively small β. As shown in Fig. 8b, the horizontal force $|F_x|$ increases monotonously at first until it reaches the maximum. kd is about 0.3, and then it decreases rapidly as kd increases. The change rule of the wave forces is similar among these cases with different β, and the horizontal wave force $|F_x|$ is larger for the relatively small β than that in the case with large β in general. We can clearly see from the figures that the wave characteristic has a significant effect on the terms of wave amplitude $|\eta|$, hydrodynamic pressure $|P|$ and wave force $|F|$. Besides, it also provides a valid reference of reducing the wave adverse effects for the design of offshore structures.

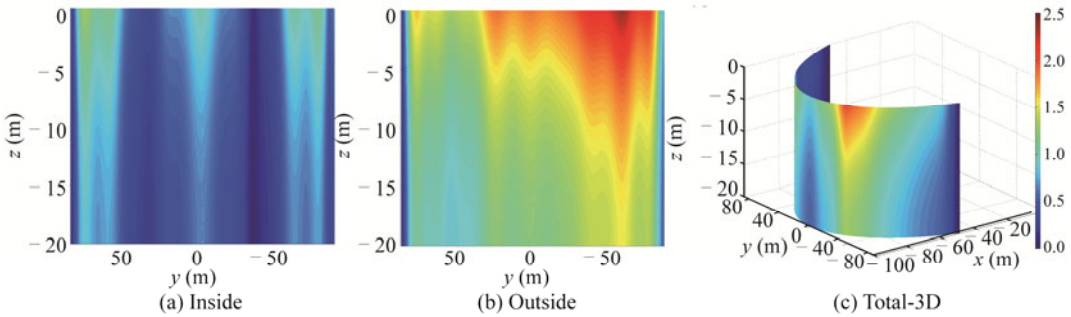

Fig. 7. Dimensionless hydrodynamic pressure on the surface of ABBW.

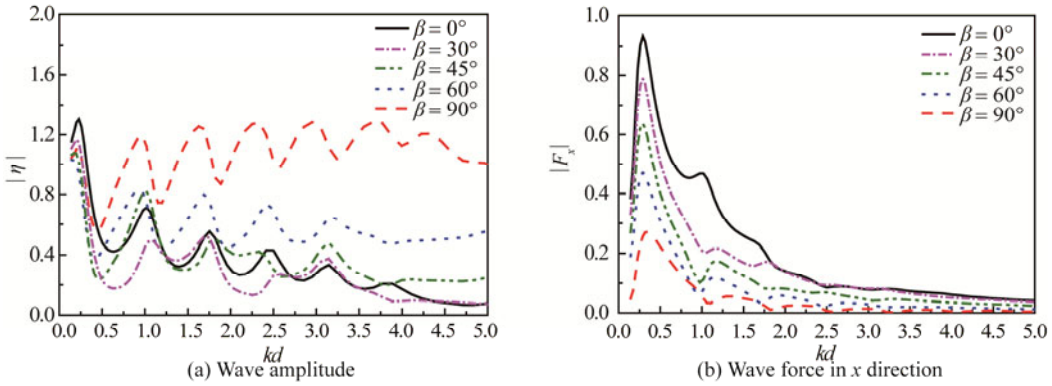

Fig. 8. Variation of the wave amplitudes at the origin and wave forces on the ABBW versus kd.

4. Conclusions

Under the assumptions of the potential flow and linear wave theory, an analytical solution has been derived and developed by an eigenfunction expansion approach to research the wave interaction with the ABBW. The results of the limiting case are compared with available study results and have an excellent agreement. Numerical results have been presented which illustrate the effects of various

wave parameters and structural configurations on the wave amplitudes distribution and the hydrodynamic loads. The ABBW can effectively affect the diffracted wave amplitude for a large opening angle whereas it affects the diffracted wave amplitude slightly for small γ, and the diffracted wave amplitudes are influenced greatly when the breakwater is against the wave of oblique incidence. The hydrodynamic pressure distribution shows that the value is larger near the free surface than that in the deep, and has a feature of symmetry for the wave normal incidence. On the other side, its distribution is asymmetrical and larger values concentrate on the upper of one side for wave oblique incidence. Further, it can be concluded that the angle between the wave incidence direction and the normal of the curved surface of the breakwater is smaller and the pressure at the same position is larger, and vice versa. The characteristic of the wave force has a similar rule with the results of the large cylinder by comparing Figs. 5b and 5d with the limiting case Fig. 2b. In general, the wave force increases rapidly at first until it reaches the maximum, and then it decreases gradually as the wavelength decreases. The opening angle γ, radius R of the breakwater and the angle of wave incidence β have a great influence on the wave force with small kd, and the horizontal wave force is relatively large when γ, d/R are large and β is small than that in the cases when γ, d/R are small and β is large. The present study can serve as a way of estimating the wave characteristics in the vicinity of the ABBW and can be used for reference in engineering design of coastal structures.

References

Bhatta, D. D. and Rahman, M., 2003. On scattering and radiation problem for a cylinder in water of finite depth, *Int. J. Eng. Sci.*, **41**(9): 931–967.

Chang, K. H., Tsaur, D. H. and Huang, L. H., 2012. Accurate solution to diffraction around a modified V-shaped breakwater, *Coast. Eng.*, **68**, 56–66.

Cheng, J. S., Miao, G. P. and Wang, J. Q., 2007. Analytical research on wave diffraction on arc-shaped bottom-mounted perforated breakwaters, *China Ocean Eng.*, **21**(3): 417–428.

Cheng, J. S., Miao, G. P., Wang, J. Q. and You, Y. X., 2006. Analytical research on the sheltering effects of arc-shaped floating breakwaters, *Journal of Shanghai Jiaotong University*, **40**(10): 1772–1777. (in Chinese)

Cheng, J. S., Miao, G. P., Wang, J. Q. and You, Y. X., 2008. Analytical research on the sheltering effect on arc-shaped bottom-mounted breakwaters, *Journal of Ship Mechanics*, **12**(1): 12–17. (in Chinese)

Duan, J. H., Cheng, J. S., Wang, J. P. and Wang, J. Q., 2012. Wave diffraction on arc-shaped floating perforated breakwaters, *China Ocean Eng.*, **26**(2): 305–316.

Garrett, C. J. R., 1971. Wave forces on a circular dock, *J. Fluid Mech.*, **46**(1): 129–139.

Kanoria, M. and Mandal, B. N., 2002. Water wave scattering by a submerged circular-arc-shaped plate, *Fluid Dyn. Res.*, **31**(5): 317–331.

Linton, C. M. and Evans, D. V., 1990. The interaction of waves with arrays of vertical circular cylinders, *J. Fluid Mech.*, **215**, 549–569.

Liu, J., Lin, G. and Li, J. B., 2012. Short-crested waves interaction with a concentric porous cylinder system with partially porous outer cylinder, *China Ocean Eng.*, **26**(2): 217–234.

Liu, J. and Lin, G., 2013. Numerical modelling of wave interaction with a concentric cylindrical system with an arc-shaped porous outer cylinder, *Eur. J. Mech. B/Fluid.*, **37**(7): 59–71.

Lu, Z. M., Miao, G. P., Zhu, R. C. and Cheng, J. S., 2007. Analytical research on the wave force exerted on

V-shaped bottom-mounted breakwaters, *Journal of Hydrodynamics, Ser. A*., **22**(1): 135−141. (in Chinese)

MacCamy, R. C. and Fuchs, R. A. 1954. *Wave Forces on Piles*: *A Diffraction Theory*, Technical Memorandum No.69, Beach Erosion Board, Washington, D.C.

Mclver, M. and Urka, U., 1995. Wave scattering by circular arc shaped plates, *J. Eng. Math.*, **29**(6): 575−589.

Miao, G. P., Cheng, J. S., Wang, J. Q. and You, Y. X., 2005. Wave diffraction on arc-shaped bottom-mounted breakwaters, *J. Hydrodyn.*, *Ser. B*., **17**(4): 391−397.

Sankarbabu, K., Sannasiraj, S. A. and Sundar, V., 2008. Hydrodynamic performance of a dual cylindrical caisson breakwater, *Coast. Eng.*, **55**(6): 431−446.

Song, H. and Tao, L., 2007. Short-crested wave interaction with a concentric porous cylindrical structure, *Appl. Ocean Res.*, **29**(4): 199−209.

Spring, B. H. and Monkmeyer, P. L., 1974. Interaction of plane waves with vertical cylinders, *Proc. 14th Int. Conf. Coast. Eng.*, Copenhagen, Denmark, **1**(14): 1828−1847.

Williams, A. N. and Li, W., 2000. Water wave interaction with an array of bottom-mounted surface-piercing porous cylinders, *Ocean Eng.*, **27**(8): 841−866.

Zhu, S. P. and Moule, G., 1994. Numerical calculation of forces induced by short-crested waves on a vertical cylinder of arbitrary cross-section, *Ocean Eng.*, **21**(7): 645−662.